The EMBO Journal (2009) 28, 3785–3798 | © 2009 European Molecular Biology Organization | All Rights Reserved 0261-4189/09
www.embojournal.org

THE EMBO JOURNAL

Molecular crowding affects diffusion and binding of nuclear proteins in heterochromatin and reveals the fractal organization of chromatin

Aurélien Bancaud[1,3,4], Sébastien Huet[1,3], Nathalie Daigle[1], Julien Mozziconacci[1], Joël Beaudouin[2] and Jan Ellenberg[1,*]

[1]Cell Biology and Biophysics Unit, EMBL, Heidelberg, Germany and [2]Deutsches Krebsforschungszentrum and BioQuant, Research Group Theoretical Bioinformatics, Heidelberg, Germany

The nucleus of eukaryotes is organized into functional compartments, the two most prominent being heterochromatin and nucleoli. These structures are highly enriched in DNA, proteins or RNA, and thus thought to be crowded. *In vitro*, molecular crowding induces volume exclusion, hinders diffusion and enhances association, but whether these effects are relevant *in vivo* remains unclear. Here, we establish that volume exclusion and diffusive hindrance occur in dense nuclear compartments by probing the diffusive behaviour of inert fluorescent tracers in living cells. We also demonstrate that chromatin-interacting proteins remain transiently trapped in heterochromatin due to crowding induced enhanced affinity. The kinetic signatures of these crowding consequences allow us to derive a fractal model of chromatin organization, which explains why the dynamics of soluble nuclear proteins are affected independently of their size. This model further shows that the fractal architecture differs between heterochromatin and euchromatin, and predicts that chromatin proteins use different target-search strategies in the two compartments. We propose that fractal crowding is a fundamental principle of nuclear organization, particularly of heterochromatin maintenance.

The EMBO Journal (2009) **28,** 3785–3798. doi:10.1038/emboj.2009.340; Published online 19 November 2009
Subject Categories: chromatin & transcription
Keywords: chromatin organization; fluorescence correlation spectroscopy; live cell fluorescence microscopy; fractal crowding; nuclear diffusion

Introduction

The interphase nucleus of eukaryotes is organized into discrete functional structures. These structures include heterochromatin, which remains condensed throughout the cell cycle, and mostly transcriptionally silent, euchromatin, which is decondensed during interphase and enriched in active genes, and nucleoli, where rRNA transcription and processing occur. They are well-characterized biochemically (Andersen *et al*, 2005), and can be observed for hours by light microscopy in living cells. Despite these stable properties, nuclear compartments are highly dynamic at the molecular level, if probed by fluorescence redistribution after using photobleach/activation techniques (Lippincott-Schwartz *et al*, 2001; Patterson and Lippincott-Schwartz, 2002) that showed rapid exchange of about every resident protein probed so far (Hager *et al*, 2002; Belmont, 2003; Phair *et al*, 2004; Beaudouin *et al*, 2006). To reconcile long-term macroscopic stability and molecular dynamics, nuclear compartments have been proposed to be self-organizing entities generated in a cooperative manner by a multitude of stereospecific short-lived interactions of their components (Misteli, 2005). Owing to the large number of components and non-linear cooperative biochemical couplings, this hypothesis is difficult to probe *in vivo*. As an alternative and not mutually exclusive model, macromolecular crowding has been suggested as a general driving force for self-organization of nuclear compartments on the basis of the osmotic manipulation of nucleoli in isolated nuclei (Hancock, 2004), and the use of hypertonic stress in intact cells (Richter *et al*, 2007).

Classical molecular crowding studies (for reviews, see Zimmerman and Minton, 1993; Minton, 1995) investigate *in vitro* biophysical and biochemical consequences of the presence of large amounts of inert co-solutes that reduce the available volume by steric interaction in a reaction medium. Molecular crowding is relevant to cells because they contain high concentrations of biological macromolecules, including proteins and nucleic acids that will act as co-solutes for any protein of interest. The nucleus is known to contain the highest macromolecular densities in the cell and to exhibit significant variations in chromatin concentration ranging from ~100 mg/ml in euchromatin (Daban, 2000) to ~200–400 mg/ml in heterochromatin (Bohrmann *et al*, 1993). Nevertheless, a role for molecular crowding in nuclear organization and function has been rarely discussed or investigated. *In vitro*, molecular crowding has been shown to significantly alter the biophysical and biochemical properties of proteins. First, crowding induces volume exclusion: the volume occupied by co-solutes is inaccessible to other proteins, reducing their apparent concentration. Second, crowding slows down diffusion up to several orders of magnitude (Muramatsu and Minton, 1988): as co-solutes act as obstacles, they hinder molecular motion with a strong dependence on obstacle connectivity (Saxton, 1993b). Third, crowding shifts binding reactions towards bound states (Minton, 1995, 1998, 2006) because the reduction in available volume induced by co-solutes favours protein configurations associated with a reduction of entropy, that is, complexes rather than individual dissociated subunits.

*Corresponding author. Cell Biology and Biophysics Unit, EMBL, Meyerhofstraße 1, Heidelberg D-69117, Germany.
Tel.: +49 6221 387 8328; Fax: +49 6221 387 89328;
E-mail: jan.ellenberg@embl.de
[3]These authors contributed equally to this work
[4]Present address: LAAS-CNRS; Université de Toulouse, 7, avenue du Colonel Roche, F-31077 Toulouse, France

Received: 14 July 2009; accepted: 19 October 2009; published online: 19 November 2009

Recent studies have shown how the dynamics of nuclear proteins is governed by their diffusion and binding properties (Sprague *et al*, 2004, 2006; Beaudouin *et al*, 2006). If molecular crowding applies in the nucleus, we expect nuclear density variations to alter protein dynamics locally and to influence nuclear organization. Although the initial formation of nuclear structures probably requires stereospecific interactions, crowding-enhanced protein association could reinforce and maintain dense nuclear compartments. Molecular crowding could thus provide a driving force to maintain nuclear compartments composed of dynamic molecules without the need for membranes or other structural boundaries. This scenario seems to be particularly relevant for heterochromatin, formation of which requires specific histone modifications that create stereospecific binding sites (Rea *et al*, 2000), but maintenance of which could be facilitated by enhancing protein binding mediated by crowding.

Several studies have shown that volume exclusion occurs in some nuclear compartments (Verschure *et al*, 2003; Gorisch *et al*, 2005) as predicted by the crowding theory, but local effects on diffusion and binding properties of nuclear proteins remain to be demonstrated *in vivo*. Here, we investigate the three consequences of molecular crowding within the nucleus of living cells. First, we demonstrate volume exclusion of inert tracers in dense nuclear compartments by high-resolution confocal imaging of their steady state concentrations. Second, we use fluorescence correlation spectroscopy to show that diffusion of these tracers is slowed down in dense nuclear compartments, although they remain kinetically permeable. Third, we demonstrate that binding rates are enhanced in dense nuclear compartments using local photoactivation (PA) of chromatin-interacting proteins.

Having demonstrated the prevalence of molecular crowding effects in the nucleus, our quantitative analysis of molecular dynamics in live-cell nuclei allowed us to define the structural organization of the main nuclear crowding agent, chromatin. Three independent lines of evidence lead us to conclude that its organization is fractal. First, chromatin obstructs diffusion of inert tracers in a size-independent manner. Second, single particle displacements of quantum dots exhibit non-random distributions at short time scales consistent with fractal obstacles. Third, the enhanced binding kinetics of chromatin-interacting proteins in heterochromatic regions are well explained by a fractal kinetics model but cannot be explained by diffusion reaction models. Our analysis allows us to determine two structural parameters of chromatin, the anomaly parameter it imposes on diffusion and the fractal dimension, which characterize the random motion of diffusing tracers and the geometrical arrangement of chromatin, respectively. Together with previously established diffusion reaction models (Beaudouin *et al*, 2006), this study provides a comprehensive framework to mathematically describe nuclear protein dynamics.

Results

Nucleoli and heterochromatin exhibit size-dependent volume exclusion

Nucleoli are the most prominent and dense nuclear subcompartments composed, among others (Andersen *et al*, 2005), of rDNA and transcription complexes, rRNA processing complexes and modification machinery, as well as assembling ribosomal subunits. The volume fraction occupied by these macromolecules is not available for other species, and we expect volume exclusion to occur. Consequently, fluorescent inert probes should be partly physically excluded from nucleoli, and exclusion should be size dependent (Zimmerman and Minton, 1993). To evaluate nucleolar volume availability, we chose NRK cells for their large and easy-to-localize nucleoli (Figure 1A), and microinjected fluorescent dextrans of different molecular weights (MW) or expressed different GFP multimers. Confirming previous studies, for example, those by Gorisch *et al* (2003) and Handwerger *et al* (2005), we found that these tracers are excluded from nucleoli (Figure 1A). We quantified the relative exclusion, defined by the nucleolar-to-nucleoplasmic concentration ratio. Relative exclusion was found to be size dependent and to increase with probe size, being two-fold greater for a particle of $\sim$90 nm in diametre (500 kDa dextran) in comparison to a particle of $\sim$20 nm (25 kDa dextran, (Lenart and Ellenberg, 2006)).

As heterochromatin is likely to be a compartment influenced by crowding effects, we assessed the behaviour of similar tracers in comparison with euchromatin. We used NIH3T3 cells in which large heterochromatin foci of about 1 μm diametre can be seen after vital DNA labelling. As previously observed (Gorisch *et al*, 2003; Verschure *et al*, 2003), we confirmed that exclusion occurs in heterochromatin (Figure 1B). For each tracer, the relative exclusion increased approximately linearly with heterochromatin concentration, and single-parameter linear fits were performed to deduce heterochromatin 'exclusion rates' (Supplementary Figure S1). Plotting tracer exclusion for heterochromatin foci for which DNA density was, for example, six times greater than euchromatin (green arrow in Figure 1B), clearly shows that the relative exclusion is size dependent, reaching $\sim$50% for 500 kDa dextrans (Figure 1B, right panel).

These experiments show that heterochromatin and nucleoli are crowded to a degree that significantly reduces the available volume although still allowing the placement of molecules of as large as $\sim$90 nm diametre.

Newly formed heterochromatin exhibits volume exclusion

To test whether heterochromatin causes volume exclusion, we induced its formation by overexpressing Suv39H1, the enzyme known to trigger heterochromatin formation by histone H3 methylation (Rea *et al*, 2000), in NRK cells that normally show a rather homogeneous chromatin pattern in interphase. DNA was vitally stained with Hoechst to monitor chromatin density, and an RFP dimer was co-expressed to serve as a volume exclusion reporter (Figure 1C).

To measure the effect of Suv39H1 expression on heterochromatin, we used quantitative analysis of the pixel intensity distribution in the DNA channel (see Supplementary Figure S1e for details), which allowed us to compute the fraction of heterochromatin per nucleus. In control cells, the chromatin organization was rather homogeneous with a low heterochromatin content of $12 \pm 2\%$ (s.e., $n = 16$) and the distribution of the volume exclusion reporter RFP dimer showed hardly any detectable region of volume exclusion (blue arrowhead in Figure 1C) apart from nucleoli. In cells overexpressing Suv39H1, many dense intra-nuclear DNA foci

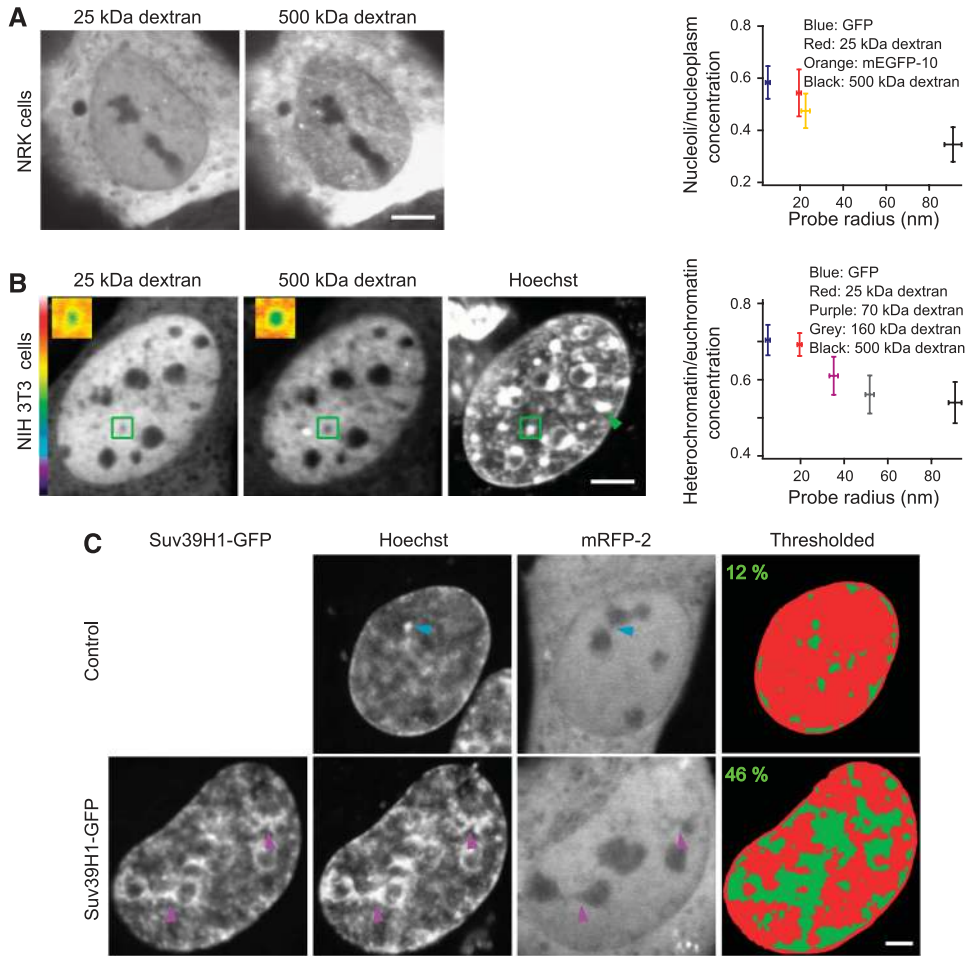

Figure 1 Steady state and induced volume exclusion in heterochromatin and nucleoli. (**A**) NRK cells were co-injected with 25 and 500 kDa fluorescently labelled dextrans. The right panel shows nucleolar versus nucleoplasmic relative exclusion of four different inert probes in NRK. (**B**) NIH3T3 cells were co-injected with 25 and 500 kDa fluorescently labelled dextrans, and stained with Hoechst to identify euchromatin or heterochromatin foci. It should be noted that heterochromatin concentration variations are amplified using Hoechst because of its sequence preference for AT-rich regions. Insets are two-fold magnified, pseudocoloured images of a heterochromatin focus. The green arrowhead indicates a heterochromatin focus, in which the DNA density is six-fold enriched in comparison with euchromatin. The relative concentration of dextrans in heterochromatin versus euchromatin was evaluated as a function of the local amount of heterochromatin in the confocal section. In the right plot, 'effective' exclusions in heterochromatin foci of density 6 (see Supplementary Figure S1 for details) are plotted for five probes of different molecular weights. (**C**) NRK cells expressing mRFP-2 alone or co-expressing Suv39H1–GFP were stained with Hoechst. Blue and purple arrowheads indicate exemplary heterochromatin foci in which mRFP-2 exclusion can be detected. On the right, the Hoechst channel is thresholded with pixels in the range 0–49, 50–134 and 134–255 represented in black, red and green, respectively.

appeared (purple arrowheads in Figure 1C), and the heterochromatin content increased almost four-fold to $46 \pm 6\%$ (s.e., $n = 16$). The concentration of the RFP dimer in these newly formed foci was $65 \pm 10\%$ that of euchromatin. Our results show that dense chromatin regions induced by the expression of Suv39H1 exhibit volume exclusion.

Diffusion is slowed down in nucleoli and heterochromatin

Molecular crowding predicts that nuclear compartments should hinder diffusion according to their density. To test this, we probed the local diffusion by fluorescence correlation spectroscopy (FCS) with a spatial precision of ~ 300 nm, sufficient to discriminate euchromatin, heterochromatin and nucleoli. To first compare nucleoli with euchromatin, we again used NRK cells and assayed the single molecule fluctuations of a GFP pentamer through the focused laser beam. The autocorrelation function (see Materials and methods section) was shifted towards longer time scales in nucleoli (Figure 2A, orange data set in right panel), indicating an increased residence time in the measurement volume due to slower diffusion in this compartment. Fitting the autocorrelation function with an anomalous diffusion model, we determined nucleoplasmic and nucleolar diffusion coefficients of the GFP pentamer as 7.7 ± 1.3 and $2.9 \pm 0.5\,\mu m^2/s$, respectively, showing that nucleolar diffusion was slowed down by a factor of ~ 3.

To compare the diffusion in heterochromatin with euchromatin, we again used NIH3T3 cells. The GFP pentamer diffusion coefficient was decreased by a factor of 1.6 from $9.2 \pm 1.0\,\mu m^2/s$ in euchromatin to $5.9 \pm 0.6\,\mu m^2/s$ in heterochromatin (Figure 2B, green data set in right panel). For reference, we also recorded diffusion in NIH3T3 nucleoli, in which GFP pentamer diffusion was reduced by three-fold to $2.3\,\mu m^2/s$, consistent with the data from NRK cells (Figure 2B, red and orange data sets in lower panel, respectively).

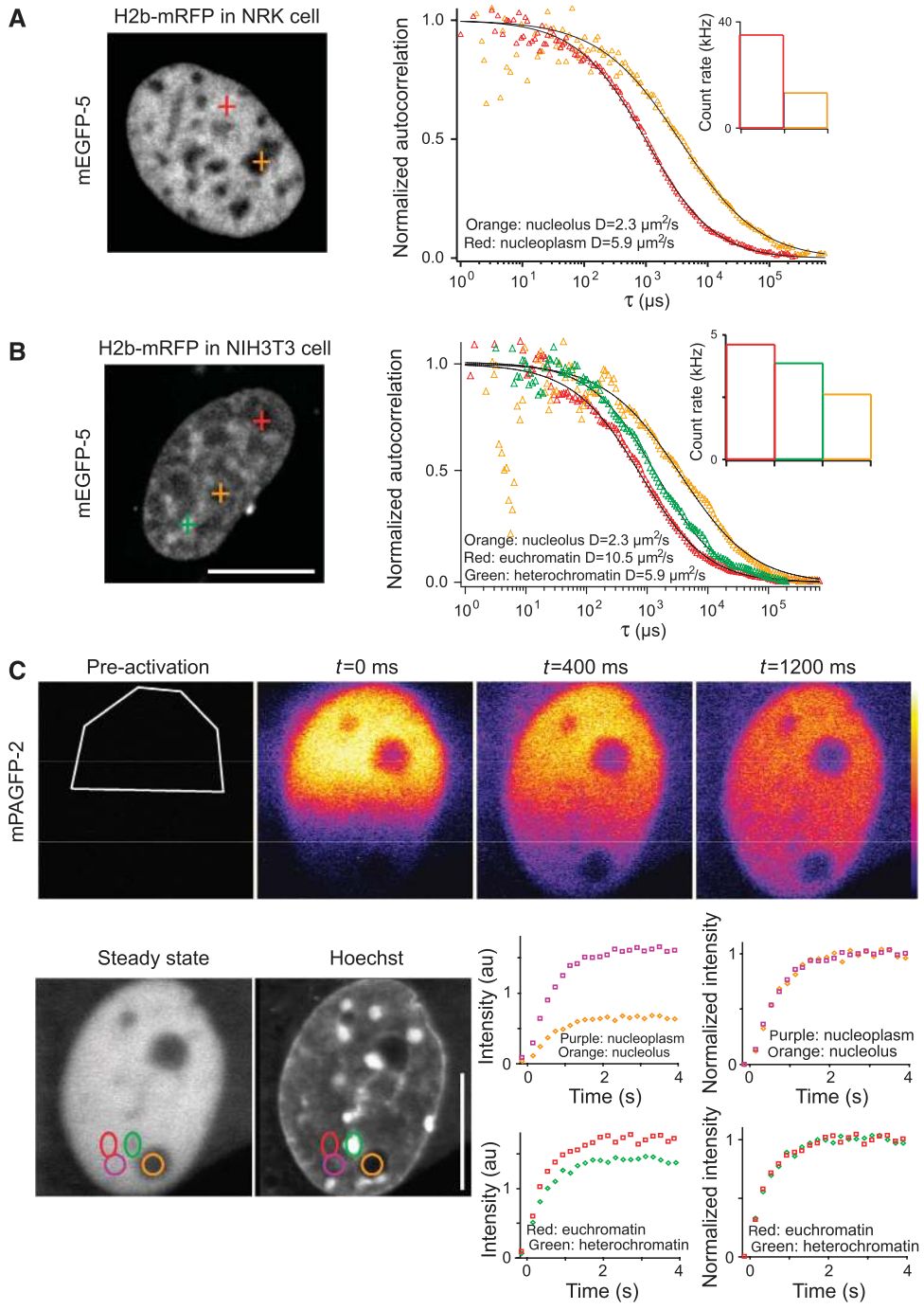

Figure 2 The nuclear rheology is heterogeneous. (**A**) NRK cell transiently expressing H2b-mRFP and mEGFP-5 were subjected to FCS measurements. Crosses on the H2b image indicate positions at which measurements were performed. The graph shows normalized auto correlation functions (ACF) obtained in the nucleoplasm (red) and the nucleolus (orange). Fits were performed with an anomalous diffusion model (solid curves), and we deduced residence times of 1050 and 3650 μs, and anomalous coefficients of 0.78 and 0.65 in nucleoplasm and nucleolus, respectively. The inset shows count rates, that is, intensities measured by FCS in the nucleoplasm (red) and nucleolus (orange). (**B**) Similar experiments performed with NIH3T3 cells. The green cross indicates the position of heterochromatin measurements, which was always quality controlled taking advantage of H2B–mRFP bleaching during FCS (Supplementary Figure S2). Graphs show normalized ACFs obtained in euchromatin (red), heterochromatin (green) and nucleoli (orange). Fits (solid curves) show more pronounced diffusion slow down in nucleoli than in heterochromatin, as inferred from the mEGFP-5 residence times of 3570 μs ($\alpha = 0.70$) and 1410 μs ($\alpha = 0.80$) in nucleoli and heterochromatin, respectively, in comparison to 790 μs ($\alpha = 0.77$) in euchromatin (bottom). Inset shows count rates measured in euchromatin (red), heterochromatin (green) and nucleoli (orange). (**C**) Selected frames of mPAGFP-2 half-nucleus PA time lapse imaging with the photoactivated region represented by the polygon on the pre-activation image. To visualize entry kinetics within nuclear compartments, 1.2-μm confocal slices were grabbed. High-quality images of mPAGFP-2 steady state and Hoechst distribution were acquired 60 s after PA (lower panel). Rings on the steady-state image correspond to regions in which the intensity redistribution was measured over time. Graphs at the left compare nucleolar (orange) and heterochromatin (green) fluorescence intensity measured over time in the regions highlighted with the corresponding coloured circles in the steady-state image to the intensity in a neighbouring nucleoplasmic area (red and purple regions). Graphs at the right display the same curves after steady-state renormalization. Scale bars 10 μm.

Our results show that crowding predictions for diffusion are relevant in the nucleus, and that diffusion is slowed down two- to three-fold in dense nuclear compartments.

Dense nuclear compartments are readily accessible for diffusing proteins

Although the concentrations of inert probes, such as GFP multimers and dextrans, were reduced in dense regions by volume exclusion, we observed only moderate diffusive hindrances in nuclear compartments, which suggest that uptake kinetics of diffusive tracers into dense compartments should not be dramatically impeded, allowing a dynamic exchange between them. To test this, we photoactivated PAGFP dimer in one-half of the nucleus and measured its fluorescence redistribution kinetics in heterochromatin or nucleoli relative to an adjacent euchromatin region (Figure 2C). As expected from our volume exclusion observations, PAGFP dimer reached lower steady state levels in nucleoli and heterochromatin (Figure 2C, left graphs). However, after steady-state normalization, all uptake kinetics seemed very similar at this temporal resolution (Figure 2C, right graphs). Thus, even the densest nuclear compartments are highly permeable, and readily accessible to diffusing proteins.

Binding to nucleosomes and DNA is enhanced in heterochromatin

The consequences of crowding on chemical reactions have been studied theoretically (Minton, 1992, 1995, 2006) and confirmed experimentally *in vitro* (e.g. Rivas *et al*, 1999, 2001). If crowding predictions apply *in vivo*, most reactions are expected to exhibit enhanced binding rates when their ligands are found in a crowded heterochromatin focus compared with less-crowded euchromatin. To test this, we assayed the behaviour of three generic chromatin-interacting proteins, the guanine nucleotide exchange factor RCC1 (Nemergut *et al*, 2001; Beaudouin *et al*, 2006), which interacts with H2A and H2B core histones; the linker histone isoform H1.1 (Brown, 2003; Beaudouin *et al*, 2006), which interacts with nucleosome entry–exit DNAs (Hamiche *et al*, 1996); and the C-terminal tail of H1.1 (H1t), which is a highly positively charged protein with an unspecific affinity for DNA (Subirana, 1990). These proteins were fused to PAGFP, and local PA in either euchromatin or heterochromatin was performed in volumes $\sim$900 nm in diametre and $\sim$3.1 μm in extension (Supplementary Figure S3a).

Consistent with our previous observations (Beaudouin *et al*, 2006), we observed a rapid and complete fluorescence redistribution of H1.1, RCC1 and H1t in euchromatin (Figure 3A, red data sets in Figure 3B), accompanied by smoothing of the local fluorescence gradient over time, which indicates a contribution of diffusion in the relaxation (Beaudouin *et al*, 2006). Using a previously established spatial diffusion reaction model (Beaudouin *et al*, 2006), we analysed our data (Supplementary data). Fitting diffusive and binding parameters to the experimental data showed that the dynamics of all three proteins in euchromatin was well explained by a diffusion-limited model (Figure 3C, red data sets and their corresponding black fitting curves). The observed redistribution kinetics are, therefore, limited by the low amount of unbound proteins in steady state rather than by the residence time on chromatin (Sprague *et al*, 2004; Beaudouin *et al*, 2006). Thus, one parameter, the fraction of unbound proteins (see Materials and methods section), suffices to describe the dynamics of these proteins and we obtained $0.2 \pm 0.1\%$ ($n = 13$), $0.9 \pm 0.1\%$ ($n = 13$) and $4.1 \pm 0.4\%$ ($n = 13$) as the free fraction for H1.1, RCC1 and H1t respectively. As binding of H1.1, RCC1 and H1t to euchromatin is short lived, we could only estimate upper limits for their residence times of $\sim$2, $\sim$0.2 and $\sim$0.1 s, respectively.

As all three proteins interact with chromatin with low specificity independent of histone modifications or DNA sequence, the same diffusion-limited approximation should be applicable to heterochromatin (green data sets in Figure 3B). As heterochromatin is enriched in nucleosomes and DNA, the binding sites for H1.1, RCC1 and H1t, we would expect to observe slowed-down kinetics linearly dependent on the heterochromatin-to-euchromatin concentration ratio. Surprisingly, all three proteins exhibited biphasic kinetics in heterochromatin with a plateau at short time scales, which indicates trapping of H1.1, RCC1 and H1t in heterochromatin. However, taking into account the higher local concentration of binding sites, the diffusion reaction model (Figure 3B, upper black curves) could not fit the redistribution kinetics observed in heterochromatin, and even further refinement by implementing the two-fold diffusion slow down and a possible enhancement of association rates in heterochromatin failed to fit the data (Supplementary Figure S3). To explicitly model crowding, we therefore turned to molecular dynamics simulations (Supplementary data) defining chromatin structure as a network of randomly distributed obstacles and binding sites with a constant binding site-to-obstacle ratio (Supplementary Figure S4). Although increasing obstacle density in heterochromatin could simulate a delayed redistribution, the random crowding model also failed to explain the biphasic kinetics observed in heterochromatin (Supplementary Figure S4).

So far, our experiments show that all three predictions of molecular crowding are fulfilled in dense nuclear compartments such as heterochromatin in living cells. Crowding leads to volume exclusion and diffusion slow down of inert macromolecules, and locally increases the binding of chromatin-interacting proteins. Interestingly, our observations that random crowding models cannot explain the kinetics of binding enhancement suggested that a non-random organization of the crowding agent underlies these effects. We therefore decided to investigate the structural organization of euchromatin and heterochromatin in more detail.

Diffusion properties are size-independent in chromatin

We first studied chromatin structure by analysing the diffusive behaviour of GFP multimers composed of 1, 2, 5 or 10 GFPs in euchromatin in more detail using FCS. All GFP multimers exhibited sub-diffusive behaviours (e.g. Figure 4A) in agreement with previous studies (Wachsmuth *et al*, 2000; Guigas *et al*, 2007). Fitting the autocorrelation functions with an anomalous diffusion model, we found that the FCS anomaly parameter was independent of the size of the GFP multimer, with a value of 0.79 ± 0.02 (Figure 4B). The degree of diffusive hindrance as compared with aqueous solution was also size independent for euchromatin; we measured by FCS that GFP and GFP dimer were slowed down from 87 ± 7 to 29.1 ± 1.5 and 55 ± 4 to $17 \pm 1\ \mu m^2/s$,

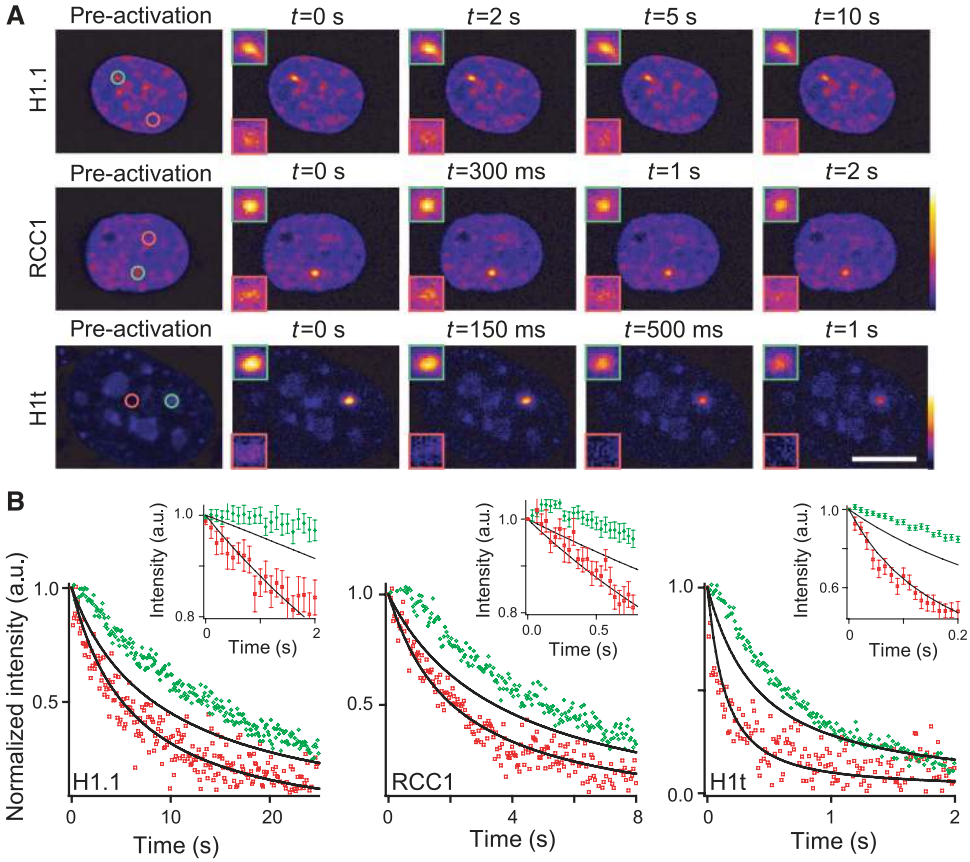

Figure 3 Binding of chromatin-interacting proteins is enhanced in heterochromatin. (**A**) Pseudocoloured images of NIH3T3 cells transiently expressing H1.1–mPAGFP, RCC1–mPAGFP and H1t–PAGFP. Images are selected frames of PA time lapse with the photoactivated region represented by circles in euchromatin (red) or in heterochromatin (green) on the pre-activation image. The inserts outlined in red and green correspond to two higher magnifications of photoactivated areas in euchromatin and heterochromatin, respectively. Two lookup tables associated to heterochromatin PA and nuclei, or to euchromatin PA are defined in the middle and lower panel, respectively. Experiments with RCC1–mPAGFP and H1t–mPAGFP were carried out at 26°C. Confocal section thickness values were set to 1.0 μm, that is, three times less than the photoactivated spot size. Scale bar 10 μm. (**B**) Graphs representing normalized intensities measured during relaxation in the circled regions of the experiment displayed in (**A**) (red: euchromatin, green: heterochromatin). Euchromatin responses are accurately fitted with a diffusion limited model (see Materials and methods section, lower solid line), but this model fails to reproduce heterochromatin response curves (upper solid lines) especially at short time scales, showing that chromatin protein dynamics are associated with a longer residence in heterochromatin right after PA. Insets represent average early time points responses measured in euchromatin and heterochromatin (red and green data sets, respectively) to emphasize on the initial plateau in heterochromatin.

respectively, by about three-fold. The size-independent nucleoplasmic diffusive hindrance is consistent with earlier studies performed with dextrans, ficolls and GFP multimers spanning a broad range of MWs (Seksek *et al*, 1997; Pack *et al*, 2006). Diffusion was also probed in heterochromatin in comparison with euchromatin, and similar diffusional hindrances of 1.7 ± 0.2 and anomaly parameters of 0.75 ± 0.07 were observed between GFP decamers, pentamers and dimers (Supplementary Figure S2), suggesting that diffusion properties were also size independent in heterochromatin. Conversely, diffusive properties were not size independent in nucleoli, in which chromatin is not the main structural component, as the anomaly parameter and the diffusive hindrance tended to decrease and increase, respectively, with MW (Supplementary Figure S2).

Chromatin structure is consistent with ~100-nm fractal domains

We then used single particle tracking of small quantum dot aggregates (QDs) to explore chromatin structure with a better spatial resolution than that of FCS, which is typically limited to ~300 nm (Figure 4C and Supplementary Figure S5a). The analysis of the mean square displacements (MSD, blue data set in Figure 4D) showed that QD motion was sub-diffusive at short time scales as their diffusion coefficient decreased with time. This sub-diffusive behaviour was characterized by an anomaly parameter $\gamma = 0.73$ (solid line in Figure 4D, see Materials and methods), in excellent agreement with the value of 0.79 obtained from FCS measurements of GFP multimers (Figure 4B). At longer time scales QD motion switched to a purely diffusive regime characterized by a linear dependence of MSD with time (Figure 4D).

To obtain more insight into the nature of the sub-diffusive behaviour, we analysed the distributions of QD displacements at different time scales (Figure 4E). For displacements longer than 20 ms, histograms were accurately fit with a random walk model (Figure 4E, cyan line and black fit; also see Supplementary Figure S5b), suggesting that chromatin is a random medium for mean displacements greater than 100 nm, the mean distance explored by QDs at this time scale. By contrast, for displacements over times shorter than 20 ms, a random walk model did not fit the distribution (Figure 4E, red line and black fit) and produced large residuals between fit and data (Figure 4E, inset), indicating

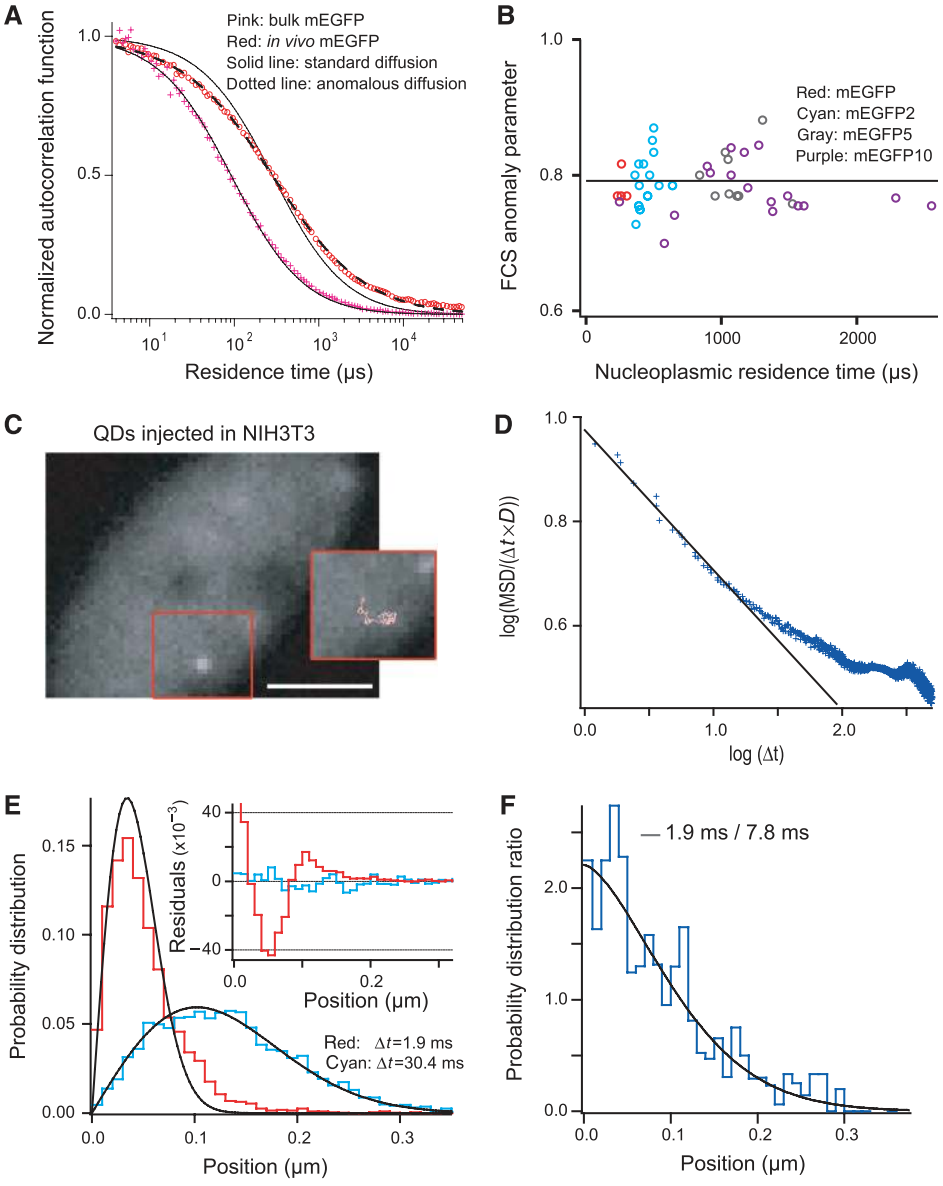

Figure 4 Chromatin shows a fractal organization at length scales $\leqslant \sim 100$ nm. (**A**) Average FCS response of mEGFP in bulk (pink crosses) fitted with a standard diffusion model ($\alpha = 1$ in equation (7)), and in the nucleoplasm (red circles) fitted with an anomalous sub-diffusive model ($\alpha = 0.79$, dashed line) or a standard diffusion model (solid line). (**B**) FCS behaviours of mEGFP (red), mEGFP-2 (cyan), mEGFP-5 (green) and mEGFP-10 (purple) multimers were probed in the nucleoplasm of NRK cells. As GFP decamers and to a lesser degree GFP pentamers were partially degraded in cells (Supplementary Figure S5), we used the residence time in the FCS volume to report their molecular weight. On the basis of anomalous sub-diffusion fits, anomalous parameters are plotted versus nucleoplasmic residence times that are assumed to be proportional to mEGFP multimers MW. (**C**) NIH3T3 cells were micro-injected with QDs. The inset shows the trajectory of one QD aggregate obtained from a time series acquired every 1.9 ms. Scale bar 5 µm. (**D**) Plot of $\log(\mathrm{MSD}/(D \times \Delta t))$ versus $\log(\Delta t)$ averaged over 16 tracks (blue crosses), and linear fit at short time scales (black line), slope of which ($\gamma = 0.73$ in equation (3)) shows the anomalous subdiffusive motion of QDs. The plateau at long time scales corresponds to a standard diffusive behaviour. (**E**) Histograms of the displacement at 1.9 ms (red) and 30.4 ms (cyan) obtained with 15 independent tracks ($\sim 14\,000$ points), and their corresponding fits based on a random walk model (equation 5). In the inset, residuals show the Brownian response at 30.4 ms (cyan), and the deviation to this behaviour at 1.9 ms (red). The discrepancy to the Brownian model at 1.9 ms was neither observed in control experiments performed in free solution nor with QDs bound to chromatin (Supplementary Figure S5), and we show in Figure S5g that this anomalous behaviour cannot be explained by QDs transiently binding to chromatin. (**F**) The blue plot shows the ratio of displacement histograms at 1.9 ms versus 7.8 ms for one QD trajectory (blue data set). The solid curve corresponds to the fit obtained with the stretched exponential model (see equation (6) in Materials and methods section). Its amplitude is related to fractal dimension of chromatin, and we measure $f = 2.5$ given that $\gamma = 0.73$. It should be noted that $f = 3.0$ in the case of free diffusion (Supplementary Figure S5).

that chromatin is non-randomly organized at length scales below 100 nm. Interestingly, such a deviation from random walk diffusion models is similar to predictions from simulations of particle motion in fractal obstacles (Saxton, 1993b).

Chromatin is by far the most likely candidate for a general nuclear crowding agent that could govern QD motion in a fractal manner. This is confirmed by our observation that inducing heterochromatin formation increases the degree of molecular crowding (Figure 1C). In addition, the fact that

both the anomaly parameter and the diffusion slow down in euchromatin and heterochromatin are size independent suggests a fractal organization of chromatin. Interestingly, nucleoli that are dominated by RNA and protein as crowding molecules do not show these size-independent effects on diffusion. Fractal structures have no characteristic length scales; so diffusing molecules will encounter the same obstructions regardless of their size (Saxton, 1993a; Netz and Dorfmüller, 1995; Fatin-Rouge *et al*, 2004), causing a constant diffusive hindrance and anomaly parameter over a broad range of MWs.

In conclusion, chromatin architecture is consistent with a fractal model at length scales smaller than $\sim$100 nm, leading to a size-independent obstruction for the vast majority of proteins or nucleoprotein complexes diffusing in the nucleus.

A fractal model explains binding kinetics in heterochromatin

The fractal model of chromatin organization derived from the rheological experiments predicts that binding reactions should exhibit fractal kinetics. We therefore tested whether fractal kinetics could explain the fluorescence redistribution data obtained in our PA experiments with three chromatin-interacting proteins (Figure 3), that we could not explain with diffusion reaction models. In a fractal medium, the anomalous diffusion as well as the architecture of the confining environment determine the encounter rate of interacting species and consequently lead to altered association rates in binding reactions (Kopelman, 1986). Reaction constants are therefore time dependent (Kopelman, 1986), and characterized by their fractal exponents ε according to:

$$k(t) \approx t^{-\varepsilon} \quad (1)$$

with $0 \leqslant \varepsilon \leqslant 1$ the fractal exponent of the reaction. Thus, fractal kinetics are intrinsically associated with maximal association rates at short times, in agreement with the enhanced residence of chromatin-interacting proteins we observed at short time scales in heterochromatin (Figure 5A, green data sets). Indeed, a fractal kinetics model could accurately reproduce the initial fluorescence redistribution in heterochromatin in contrast to the reaction diffusion model (compare upper cyan fit curves in Figure 5A with upper black fit curves in Figure 3C). In heterochromatin, we obtained fractal exponents ε of 0.14 ± 0.07, 0.34 ± 0.14 and 0.13 ± 0.05 for H1.1, RCC1, and H1t, respectively. In some cases for H1.1, RCC1 or H1t, the relaxation curves could not be fit with the fractal kinetics model at long time scales (upper cyan fit curve in Figure 5A 'RCC1'), suggesting that the fractal exponent ε may decrease with time. This is in agreement with the observation that the QD motion enters a purely diffusive regime at long time scales (Figure 4C). For euchromatin, the fractal exponent was lower than 0.01 in all three cases (lower cyan fit curves in Figure 5A) but the fractal kinetics model reproduced experimental observations with accuracy similar to the reaction diffusion model (compare lower fit curves in Figures 3C and 5A).

Our results show that the dynamics of chromatin-interacting proteins are consistent with fractal binding kinetics. Together with the size-independent diffusion hindrance and anomaly parameter of GFP multimers and the sub-diffusive behaviour of QDs at short time scales, three independent lines of evidence, therefore, support a fractal working model of chromatin architecture as the main crowding agent in the nucleoplasm.

The fractal dimension of chromatin ranges from 2.2 to 2.6

Displacement distributions reflect the motion of QDs in their surrounding environment. In fractal media their profiles should depend on two parameters, the anomaly parameter γ and the fractal dimension f ((Ben-Avraham and Havlin, 2000), see Materials and methods). The anomaly parameter was independently determined with FCS of GFP multimers and the MSD analysis of QDs to very similar values of 0.79 or 0.73, respectively. To also determine the fractal dimension that quantifies the roughness of the self-similar pattern and to what extent chromatin surface fills its embedding volume, we further analysed the QD displacement distributions by computing the ratio of distributions at 1.9 versus 7.8 ms (see Materials and methods), and we deduced that the fractal dimension of chromatin was $f \sim 2.61 \pm 0.15$ on the basis of single parameter fits of 68 QD tracks ($n = 5$ cells, Figure 4F).

PA, FCS and SPT data provides additional insights on the fractal dimension of chromatin in live cells. Indeed, the fractal dimension is also related to the fractal exponent ε characterizing fractal kinetics (Eq. 1) and the anomaly coefficient of the diffusion as follows (Kopelman, 1986):

$$f = \frac{2(1-\varepsilon)}{\gamma} \quad (2)$$

In euchromatin, we obtained a low fractal exponent $\varepsilon \sim 0$ from modelling PA unbinding kinetics and an anomaly coefficient of diffusion $\gamma = 0.76 \pm 0.03$ from FCS and SPT measurements of inert tracers leading to $f \sim 2.6 \pm 0.1$, in excellent agreement with the previous measurement. Given that we obtained the same anomaly coefficient for heterochromatin in our FCS experiments but a higher fractal exponent of $\varepsilon \sim 0.18 \pm 0.05$ in PA experiments, the fractal dimension of heterochromatin is $\sim 2.2 \pm 0.2$.

Thus, the fractal architecture of chromatin seems to be modulated in nuclear compartments with a fractal dimension that is larger in euchromatin than in heterochromatin, suggesting that chromatin exposes a large surface to nuclear proteins in this transcriptionally active compartment.

Discussion

Molecular crowding has a key role in nuclear architecture

In this study, we investigated the interplay between nuclear architecture and diffusive and binding properties of nuclear macromolecules in live cells. We showed that crowding, which causes volume exclusion, diffusive hindrance and enhanced affinity in dense nuclear compartments, dictates the behaviour of nuclear proteins. As this mechanism requires dense structures to be already assembled, it cannot replace stereospecific interactions (e.g. HP-1 binding to histones methylated by Suv39-H1 in heterochromatin (Rea *et al*, 2000; Cheutin *et al*, 2003)), but it will reinforce such interactions locally. We thus propose molecular crowding as a force that promotes and stabilizes the self-organization of nuclear compartments (Madden and Herzfeld, 1993; Marenduzzo *et al*, 2006; Iborra, 2007; Richter *et al*, 2008). Once a sub-compartment starts to form by stereospecific

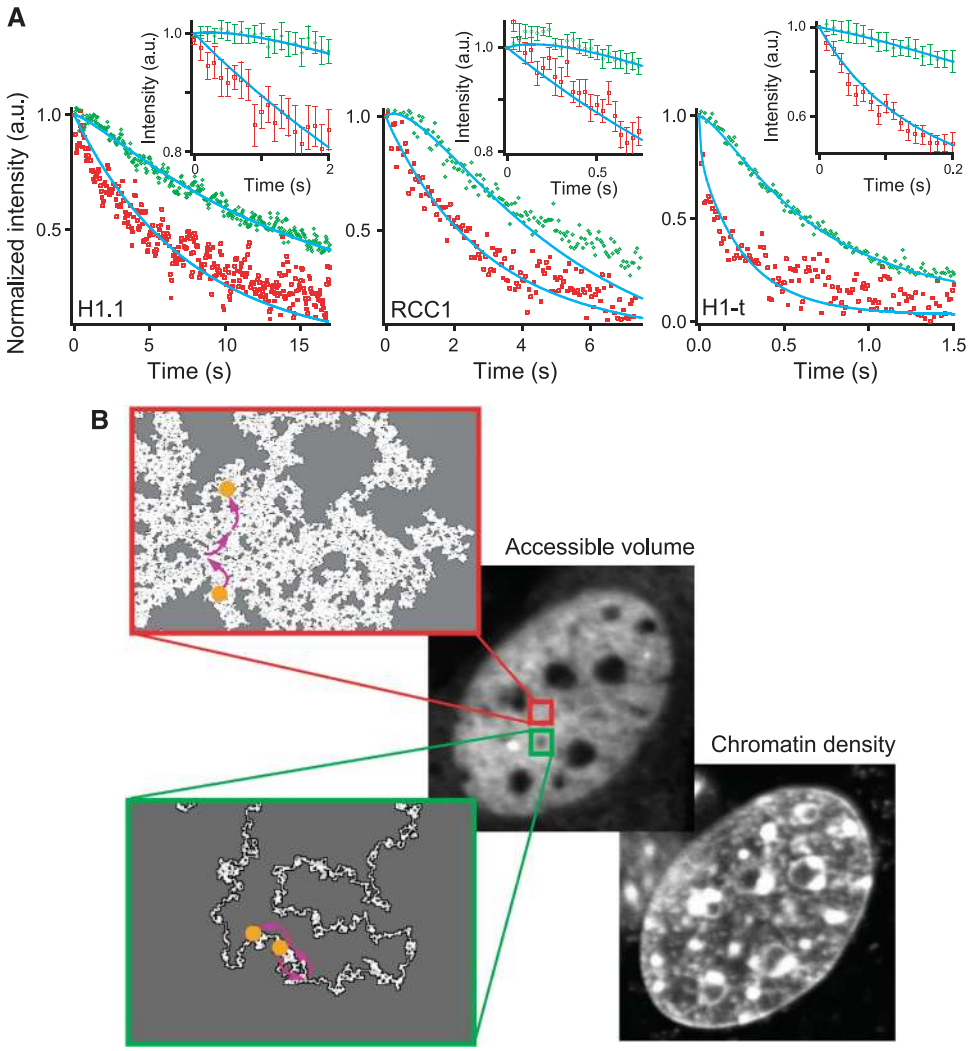

Figure 5 Fractal kinetics occur in heterochromatin. (**A**) Plots of the same H1.1, RCC1 and H1t redistributions as in Figure 3C (red and green data sets correspond to euchromatin and heterochromatin, respectively). The initial plateau can be fitted using a fractal kinetics model (upper cyan curves) with fractal exponents of 0.13, 0.39 and 0.21 for H1.1, RCC1 and H1t, respectively. Fractal exponents seemed to be lower than 0.01 in euchromatin (lower cyan curves). Insets represent average early time-point responses measured in euchromatin and heterochromatin (red and green data sets, respectively) and their corresponding fits with a fractal model (cyan curves). (**B**) 2D representation of fractal structures with two different fractal dimensions. The upper picture corresponds to a percolation cluster with $f = \sim 1.9$, and the lower one to a self-avoiding random walk with $f = \sim 1.3$. it should be noted that the upper and lower limits of self-similarity are not represented with relevant scales, and that the fractal dimension is lower than what is due because these representations are in 2D. The accessible space (white surface) and the fractal contour (black boundary) are much larger in the upper picture, as deduced in the case of euchromatin versus heterochromatin. Notably, heterochromatin compact exploration is bound to the high level of confinement in this compartment, which constrains diffusion and favours the systematic visit of its binding sites, as shown with the cartooned purple trajectories of the orange tracer.

interactions, the resulting crowding confinement would promote its maintenance by displacing chemical equilibria of interacting proteins towards bound states. This enhancement of molecular interactions by a self-governed biophysical process is generic and independent of any specific biological function or structure of the interactors. It could therefore promote maintenance of compartments at low cellular energy cost and without the need for discrete compartment boundaries such as membranes.

Even the densest nuclear compartments are highly accessible

We showed that a significant volume fraction in heterochromatin and nucleoli is not accessible to other species and causes volume exclusion. We also demonstrated that volume exclusion is associated with a moderate two- to three-fold diffusive hindrance, and that proteins enter nuclear compartments with fast dynamics. These observations can be explained by a simple crowding model, in which the nucleus is defined as a crowded organelle containing local membraneless compartments with different densities of static randomly arranged obstacles (Supplementary data). Using molecular dynamics simulations, this model was successfully tested to reproduce our observations of rapid uptake kinetics and steady-state concentration variations in dense nuclear compartments (Supplementary Figure S4a). This model also suggests that the steady-state compensated concentration, which is defined by the number of particles per unit of obstacle-free space, is homogeneous in the nucleus (Supplementary Figure S4b). From a diffusion point of

view, the homogeneous compensated concentration defines the nucleus as an organelle globally accessible to moving molecules. This applies not only to inert probes but also to proteins that interact with the obstacles. Interacting proteins are chemically partitioned at steady state into bound or unbound pools, and the diffusion laws governing the motion of the unbound pool are similar to those of inert probes such as GFP (Beaudouin *et al*, 2006). Consequently, the unbound pool is expected to spread freely into nuclear compartments and visit the entire nucleus. Notably, it is often assumed that the density in heterochromatin makes it inaccessible to RNA polymerase complexes, thereby maintaining this compartment in a transcriptionally silent state. This view is inconsistent with our observation of rapid permeation of even large diffusive tracers into heterochromatin and the only moderate diffusive hindrance they experience therein. Volume inaccessibility at the scale of an entire nuclear sub-compartment, such as nucleoli or a heterochromatin focus, is therefore conceptually insufficient to explain the transcriptional state of nuclear compartments.

Chromatin architecture is consistent with a fractal model: heterochromatin fills space more compactly than euchromatin

Chromatin structure is expected to consist of dynamic pores occurring at multiple length scales. Indeed, pores can exist within chromatin fibres due to its internal dynamics at the nucleosomal level (Bancaud *et al*, 2006), through chromatin loops that are either stabilized by protein complexes (Woodcock and Dimitrov, 2001) or occur spontaneously due to low persistence length of the fibre (Cui and Bustamante, 2000), and through chromatin interminglement (Lieberman-Aiden *et al*, 2009). Hence, chromatin organization seems to be fractal, in agreement with the well-established fractal architectures of polymer solutions (Witten, 1998). The fractal nature of chromatin has already been observed at small length scales on the basis of neutron scattering of erythrocyte nuclei (Lebedev *et al*, 2005), and suggested on the basis of FCS experiments (Wachsmuth *et al*, 2000). Chromatin structure therefore cannot be described by a typical pore size (Gorisch *et al*, 2005), but should rather be characterized by the fractal dimension *f*, which has not been experimentally investigated so far. The *f* value spans from 2 to 3: when $f=2$, surfaces appear smooth and regular, and occupy a small fraction of their embedding volume, whereas $f=3$ corresponds to fractals that completely fill space, offering rough and large surfaces (Figure 5B).

Our live-cell measurements do not provide a direct visualization of chromatin fractal architecture (visualizing chromatin topology under physiological conditions at high resolution is currently not possible by any method we are aware of), rather we obtained three independent lines of evidence that allow us to determine the fractal dimension of euchromatin to 2.2 and heterochromatin to 2.6. Thus, euchromatin seems to have a rougher fractal structure compared with relatively smoother heterochromatin, in agreement with structural models of metaphase chromosomes, which predict that chromatin decondensation would cause an increase in fractal dimension and thus roughness (Takahashi, 1989).

What are the implications of a fractal organization of chromatin for nuclear processes *in vivo*? First, the imposed moderate diffusion hindrance by chromatin will be size independent up to a scale of $\sim$100 nm and should, therefore, allow most biological macromolecules and even large multiprotein complexes to visit the entire nucleus to find targets or interactors. Second, the difference in fractal dimension between euchromatin and heterochromatin could influence the accessibility of DNA. Euchromatin with its larger fractal dimension will be rougher probably offering more exposed DNA at its surfaces. More accessible DNA surfaces can be scanned more efficiently by nuclear factors than in heterochromatin, therefore, favouring active transcription. In contrast, heterochromatin that fills space more compactly probably offers less exposed DNA at its surface, which is therefore less accessible to scanning by transcription factors, favouring a transcriptionally silent state. Although the model of a fractal organization of chromatin is consistent with all our observations, it certainly has limitations and will require future validations and refinements. For example, using photoactivated localization microscopy (Betzig *et al*, 2006) applied to cells expressing core histones tagged with photoswitchable fluorophores could provide structural information on chromatin with nanometer precision.

A comprehensive framework for understanding nuclear protein dynamics can be constructed on the basis of fractal organization of chromatin

The mobility of molecules in fractal structures is characterized by two parameters (Ben-Avraham and Havlin, 2000), namely the fractal dimension *f* of the confining environment and the anomaly coefficient γ of diffusion. Such a fractal model accounts for our experimental measurements of the volume exclusion and the diffusive hindrance. First, in a fractal environment, the accessible fraction of the total volume (Φ) solely depends on the fractal dimension, and on the upper (H) and lower (h) length limits of self-similarity (Supplementary data). In euchromatin, we obtain an accessible volume fraction of $27\pm8\%$ given that $f=\sim2.61$, $H=\sim100$ and $h=\sim3$ nm, which corresponds to the smallest probe used in this report and is similar to the dimension of single nucleosomes. Polymer physics predicts that the upper length limit of self-similarity should decrease non-linearly with density (Supplementary data). As heterochromatin foci are typically $\sim$two-fold denser than euchromatin, we expect $H=\sim60$ nm. Thus, we obtain accessible volume fraction of $11\pm6\%$ in heterochromatin. From these estimations, we predict that heterochromatin exclusion relative to euchromatin, as defined in Figure 1B, should be $27/12\sim2$ fold, in agreement with our measurements of steady state concentration differences of inert tracers in these two compartments.

The accessible volume fraction can independently be derived from the diffusive hindrance using a rheological approach (Neale and Nader, 1974), which describes chromatin as a porous material containing a swarm of spherical particles of arbitrary size distribution (Supplementary data). Experimentally, we measured D/D_0 of 0.3 and 0.17 in euchromatin and heterochromatin, respectively, leading to porosities of $\Phi=39\pm5$ and $23\pm4\%$, respectively, which are consistent with the fractal model predictions. In addition, the accessible volume fraction in a 150-mg/ml DNA solution, which represents a concentration relatively similar to that in euchromatin, was estimated to be in the same range of magnitude $\sim35\%$ (Strzelecka and Rill, 1987).

Table I Chromatin structural parameters are measured by [a]SPT, [b]FCS, [c]fractal kinetics in PA experiments, and [d,e,f]polymer physics considerations, fractal structural properties and rheological considerations, respectively (data)

	Euchromatin	Heterochromatin
Anomalous diffusion coefficient (γ)	$0.73^{a}/0.79^{b}$	0.77 ± 0.03^{b}
Fractal dimension (f)	$2.6 \pm 0.2^{a,c}$	2.2 ± 0.2^{c}
Upper limit of self similarity (H)	100 nm	60 nm[d]
Lower limit of self similarity (h)	3 nm	3 nm
Fractal exponent (ε)	$<0.01^{c}$	0.18 ± 0.05^{c}
Accessible to total volume ratio (Φ)	0.39 ± 0.05^{f}	0.25 ± 0.04^{e}
	0.24 ± 0.04^{f}	0.11 ± 0.06^{e}
Diffusive hindrance (D/D_0)	0.3 ± 0.03^{b}	0.17 ± 0.03^{b}

Taken together, the fractal description of chromatin provides a comprehensive theoretical framework that explains all our experimental observations (Table I). The fact that the binding kinetics of chromatin-interacting proteins is significantly changed in heterochromatin due to the architecture of this compartment (Figure 5A) highlights the importance of the fractal nature of chromatin for understanding nuclear protein dynamics.

A new model for chromatin self-organization

Interestingly, the fractal model of chromatin can also be used to predict how generic and sequence-specific interactors will find their target sites in chromatin. Our measurements show that the product of the fractal dimension and the anomaly coefficient $f \times \gamma$ is ~ 1.7 in heterochromatin, that is, lower than 2. Moving in a confining environment with such characteristics will occur in a regime termed 'compact exploration' (Condamin *et al*, 2007; Guigas and Weiss, 2008). In compact exploration, proteins located in heterochromatin compartments will systematically visit neighbouring binding sites before exiting the compartment. Compact exploration thus accounts for the plateau in unbinding kinetics we observed at short time scales in heterochromatin, (Figure 3C) because chromatin-interacting proteins bind to many sites and hence will initially remain trapped immediately after being highlighted by PA. More generally speaking, compact exploration in heterochromatin would allow chromatin-modifying enzymes to maintain epigenetic marks at a high local concentration despite the transient nature of their binding to and the high permeability of heterochromatin. In euchromatin, $f \times \gamma$ is ~ 2, corresponding to the transition between the regimes of compact and non-compact exploration. Non-compact exploration allows efficient sampling of large volumes, facilitating the search for rare or distant target sites probably required by transcription factors (purple trajectories in Figure 5B).

In summary, we propose that the differences in chromatin organization between euchromatin and heterochromatin could be maintained by a positive feedback mechanism between fractal crowding of chromatin and the activity of chromatin interactors. In this model, heterochromatinizing enzymes, such as Suv39-H1 (Rea *et al*, 2000; Cheutin *et al*, 2003), cause compaction and thus lower the fractal dimension of chromatin leading to a compact exploration scheme that in turn makes the local binding to nearby nucleosomes even more efficient. By contrast, transcription factors can find rare and distant targets by non-compact exploration in euchromatin that has a higher fractal dimension. The activity of transcription and the associated machinery keeps chromatin open and, therefore, in turn makes scanning by other transcription factors more efficient. It will be very interesting in future studies to understand the balance between these two regimes and how transitions between them are regulated.

Materials and methods

Fluorescent protein constructs and fluorescent markers

The coding sequence of pmEGFP, pPAGFP, pmPAGFP (Patterson and Lippincott-Schwartz, 2002; Lippincott-Schwartz and Patterson, 2003) and mRFP (Shu *et al*, 2006) were used to generate multimers of fluorescent proteins. Between two proteins in a tandem, the last lysine residue of the first protein has been exchanged for a glycine. For mEGFP10, two mEGFP5 multimers were fused, generating an ARPPVAT linker in between. The mRFP has been sub-cloned in place of EGFP in pEGFP-N1 (Clontech Laboratories) to allow expression in mammalian cells. RCC1 and H1.1 tagged with PAGFP have been described previously by Beaudouin *et al* (2006), and the C-terminal tail of H1.1 (H1t, 70 last amino acids) was fused to PAGFP. Suv39H1 constructs were a generous gift from JM Peters. The GFP was purchased as recombinant purified protein from Clontech Laboratories, or obtained along with GFP-2 in 100-fold diluted crude extracts after protein expression in *Escherichia coli*. Different sized dextran fractions were purchased either in fluorescently labelled form (160 kDa TRITC, Sigma-Aldrich) or as amino derivatives that were subsequently labelled (25 kDa Alexa Fluor 488, 25 kDa TRITC, 70 kDa Cy5, 500 kDa TRITC (Molecular Probes; (Lenart and Ellenberg, 2006)). Hoechst 33342 (Sigma-Aldrich) was used at a concentration of 0.5 μg/ml and added to cells at least 30 min before imaging.

Cell culture, transfection and microinjection

Normal rat kidney (NRK) cells and mouse Swiss NIH embryonic fibroblast (NIH 3T3) were cultured as described previously (Ellenberg *et al*, 1997). Cells stably expressing fluorescent fusion proteins were selected according to standard protocols and maintained in 0.5 mg/ml G418. Transfections were done with FuGene 6 (Roche) at least 48 h before imaging. For imaging, growing medium was replaced by CO_2-independent medium without phenol red (Invitrogen). Aphidicolin (5 μg/ml; Sigma) was used to synchronize NRK cells at the beginning of S-phase. Intranuclear microinjection of proteins, dextrans and QDs were performed with Femtotips II needles using an InjectMan NI 2 (Eppendorf). The 25-kDa dextran was systematically injected to serve as internal reference.

Imaging and photoactivation

Imaging was done at 37°C, unless stated, on a customized ZEISS LSM510 Axiovert confocal microscope, as described previously (Ellenberg *et al*, 1997), and a ZEISS LSM5LIVE using a $\times 63$ Plan-Apochromat 1.4 numerical aperture (NA) oil immersion or a $\times 100$ Plan-Apochromat 1.45 NA oil immersion objective lens (Carl Zeiss MicroImaging). Unless stated, 1.2-μm confocal slices were acquired to achieve nuclear compartment resolutions. Image treatment was performed using ImageJ (http://rsb.info.nih.gov/ij/); background was subtracted, intensity was normalized to the total intensity, and photophysics effects were compensated in the case of interaction kinetics (see Supplementary Figure S3 for details). Images were registered using an algorithm available on http://bigwww.epfl.ch/thevenaz/turboreg/ (Thévenaz *et al*, 1998) when required.

For tracking experiments, QDs were microinjected in nuclei and their 2D trajectories were reconstructed using the Particletracker ImageJ plugin with different kernel sizes (version 1.5, http://weeman.inf.ethz.ch/particletracker/, (Sbalzarini and Koumoutsakos, 2005)). Only continuous tracks longer than 250 frames and characterized by diffusion coefficients of $D = \sim 0.5\,\mu m^2/s$ were considered (Supplementary Figure S5). The MSD values were computed, and fitted according to:

$$\mathrm{MSD} \propto D\Delta t^{\gamma},\ \gamma < 1 \qquad (3)$$

Using the logarithm in equation (3) leads to:

$$\log(\mathrm{MSD}/(D\Delta t)) \propto (\gamma - 1) \times \log(\Delta t) \quad (4)$$

We also analysed QDs displacement histograms at various fixed time scales that were fitted with the standard Brownian diffusion model (Saxton, 1993b):

$$P(r,t) = \frac{r}{2Dt} \exp\left\{-\frac{r^2}{4Dt}\right\} \quad (5)$$

or with the stretched exponential model, which is relevant for fractal environments in the short time regime (Ben-Avraham and Havlin, 2000):

$$P(r,t) = P_0 \frac{r}{t^{\frac{\gamma}{2}(f-1)}} \exp\left\{-\left[\frac{r}{4Dt^{\frac{\gamma}{2}}}\right]^{\frac{1}{1-\frac{\gamma}{2}}}\right\} \quad (6)$$

where γ is the anomaly coefficient, which is determined by the MSD analysis. The amplitude of this function depends on P_0 and on the fractal dimension f. To remove P_0, we computed the probability distribution function of individual trajectories and calculated the ratio at two time points, and then extracted f.

Modelling PA experiments

PA experiments were analysed *in silico* running 2D computer simulations on the basis of ODE, as described previously (Beaudouin *et al*, 2006). In this approach, chromatin-interacting proteins are either interacting with chromatin, or freely diffusing, and these two states are at chemical equilibrium. Three parameters determine nuclear protein dynamics, namely their diffusion coefficients, and their association and dissociation rates in the binding reaction. Owing to the complex cellular geometry, this diffusion–reaction problem cannot be solved analytically, but numerical solutions can be obtained using, for example, the Berkeley Madonna solver (www.berkeleymadonna.com). We also tested the occurrence of fractal kinetics that have been observed in fractal environments at steady state (Kopelman, 1986). The detailed implementation of normal and fractal kinetics on the basis of Zipf–Mandelbrot distributions (Schnell and Turner, 2004) using the Berkeley Madonna solver is provided in Supplementary data.

Random models of chromatin organization were tested by running 2D molecular dynamics simulations in Matlab (www.mathworks.com), defining 640×400 pixels grids, as in for example, the study by Schnell and Turner (2004). The fraction of obstacles was kept at 30% in euchromatin and 60% in heterochromatin, and we could increase the fraction of obstacles from 0 to 100% to investigate molecular crowding consequences.

Fluorescence correlation spectroscopy

The FCS experiments were carried out at room temperature on a Zeiss Confocor 2 Laser Scanning Microscope using a $\times 40$ C-Apochromat 1.2. NA water immersion objective. They were performed at specific locations by exciting at 488 nm and collecting with a 505–550-nm pass-band filter that was suitable to avoid crosstalks with mRFP (data not shown). The FCS signal was measured at least two times consecutively per location with acquisitions times ranging from 10 to 25 s. The ACFs of these signals were computed by the Confocor interface.

For nuclear diffusion in a volume characterized by axial and equatorial radii r_0 and z_0, respectively, the normalized ACF is given by (Wachsmuth *et al*, 2000):

$$ACF = \frac{1}{\left(1 + \left(4D \times \frac{\tau}{r_0^2}\right)^{\alpha}\right) \times \left(1 + \frac{r_0^2}{z_0^2}\left(4D \times \frac{\tau}{r_0^2}\right)^{\alpha}\right)^{0.5}} \quad (7)$$

where α is the anomaly parameter ($\alpha < 1$, for sub-diffusive behaviors), and D the diffusion coefficient. α can be made equal to the anomaly parameter γ by defining the appropriate diffusion coefficient (Wu and Berland, 2008). The confocal volume aspect ratio is defined by $S = z_0/r_0$; it depends on the optical settings, and it was set to 5 in our case. The lateral residence time is $\tau_S = r_0^2/4D$. τ_S can be used to deduce any protein nucleoplasmic diffusion coefficient given EGFP FCS residence time in bulk (95 ± 8 μs), and EGFP bulk diffusion coefficient at room temperature ($87\ \mu m^2/s$; (Swamithan *et al*, 1997)). ACFs fitting was performed using Igor Pro (www.wavemetrics.com) based on equation (7), that is neglecting the contribution of EGFP photophysics (see e.g. (Wachsmuth *et al*, 2000)), to minimize the number of fitting parameters.

Western blotting

At 24 h after plasmid transfection, cells were imaged with a $\times 20$ oil immersion objective. They were then washed in PBS buffer and lysed in Laemmli loading buffer. Crude extracts were immediately placed at 95°C for 20 min and subsequently stored at −20°C until subjected to electrophoresis. For immunoblotting, membranes were incubated with an anti-GFP antibody (Roche #11814460001;1:1000), followed by incubation with an anti-mouse Alexa-680-labelled secondary antibody (Molecular Probes). Blots were scanned using the Odyssey Infrared Imager.

Supplementary data

Supplementary data are available at *The EMBO Journal* Online (http://www.embojournal.org).

Acknowledgements

We thank JM Victor and O Bénichou for stimulating discussions and critical reading, and Péter Lénárt for dextran purification and characterization. This study was supported by FEBS, EMBO and BioMS (fellowship funding to AB, SH and JB, respectively).

Conflict of interest

The authors declare that they have no conflict of interest.

References

Andersen JS, Lam YW, Leung AK, Ong SE, Lyon CE, Lamond AI, Mann M (2005) Nucleolar proteome dynamics. *Nature* **433:** 77–83

Bancaud A, Conde e Silva N, Barbi M, Wagner G, Allemand JF, Mozziconacci J, Lavelle C, Croquette V, Victor JM, Prunell A, Viovy JL (2006) Structural plasticity of single chromatin fibers revealed by torsional manipulation. *Nat Struct Mol Biol* **13:** 444–450

Beaudouin J, Mora-Bermudez F, Klee T, Daigle N, Ellenberg J (2006) Dissecting the contribution of diffusion and interactions to the mobility of nuclear proteins. *Biophys J* **90:** 1878–1894

Belmont A (2003) Dynamics of chromatin, proteins, and bodies within the cell nucleus. *Curr Opin Cell Biol* **15:** 304–310

Ben-Avraham S, Havlin S (2000) *Diffusion and Reactions in Fractals and Disordered Systems*. Cambridge: Cambridge University Press

Betzig E, Patterson GH, Sougrat R, Lindwasser OW, Olenych S, Bonifacino JS, Davidson MW, Lippincott-Schwartz J, Hess HF (2006) Imaging intracellular fluorescent proteins at nanometer resolution. *Science* **313:** 1642–1645

Bohrmann B, Haider M, Kellenberger E (1993) Concentration evaluation of chromatin in unstained resin-embedded sections by means of low-dose ratio-contrast imaging in STEM. *Ultramicroscopy* **49:** 235–251

Brown DT (2003) Histone H1 and the dynamic regulation of chromatin function. *Biochem Cell Biol* **81:** 221–227

Cheutin T, McNairn AJ, Jenuwein T, Gilbert DM, Singh PB, Misteli T (2003) Maintenance of stable heterochromatin domains by dynamic HP1 binding. *Science* **299:** 721–725

Condamin S, Bénichou O, Tejedor V, Voituriez R, Klafter J (2007) First-passage times in complex scale-invariant media. *Nature* **450:** 77–80

Cui Y, Bustamante C (2000) Pulling a single chromatin fiber reveals the forces that maintain its higher-order structure. *Proc Natl Acad Sci USA* **97:** 127–132

Daban JR (2000) Physical constraints in the condensation of eukaryotic chromosomes. Local concentration of DNA versus linear packing ratio in higher order chromatin structures. *Biochemistry* **39:** 3861–3866

Ellenberg J, Siggia ED, Moreira JE, Smith CL, Presley JF, Worman HJ, Lippincott-Schwartz J (1997) Nuclear membrane dynamics and reassembly in living cells: targeting of an inner nuclear membrane protein in interphase and mitosis. *J Cell Biol* **138:** 1193–1206

Fatin-Rouge N, Starchev K, Buffle J (2004) Size effects on diffusion processes within agarose gels. *Biophys J* **86:** 2710–2719

Gorisch SM, Richter K, Scheuermann MO, Herrmann H, Lichter P (2003) Diffusion-limited compartmentalization of mammalian cell nuclei assessed by microinjected macromolecules. *Exp Cell Res* **289:** 282–294

Gorisch SM, Wachsmuth M, Toth KF, Lichter P, Rippe K (2005) Histone acetylation increases chromatin accessibility. *J Cell Sci* **118:** 5825–5834

Guigas G, Kalla C, Weiss M (2007) Probing the nanoscale viscoelasticity of intracellular fluids in living cells. *Biophys J* **93:** 316–323

Guigas G, Weiss M (2008) Sampling the cell with anomalous diffusion—the discovery of slowness. *Biophys J* **94:** 90–94

Hager GL, Elbi C, Becker M (2002) Protein dynamics in the nuclear compartment. *Curr Opin Genet Dev* **12:** 137–141

Hamiche A, Schultz P, Ramachrisnan V, Oudet P, Prunell A (1996) Linker histone dependent DNA structure in linear mononucleosome. *J Mol Biol* **257:** 30–42

Hancock R (2004) A role for macromolecular crowding effects in the assembly and function of compartments in the nucleus. *J Struct Biol* **146:** 281–290

Handwerger KE, Cordero JA, Gall JG (2005) Cajal bodies, nucleoli, and speckles in the *Xenopus* oocyte nucleus have a low-density, sponge-like structure. *Mol Biol Cell* **16:** 202–211

Iborra FJ (2007) Can visco-elastic phase separation, macromolecular crowding and colloidal physics explain nuclear organisation? *Theor Biol Med Model* **12:** 4–15

Kopelman R (1986) Rate processes on fractals: theory, simulations and experiments. *J Stat Phys* **42:** 185–200

Lebedev DV, Filatov MV, Kuklin AI, Islamov AK, Ketzinger E, Pantina R, Toperverg BP, Isaev-Ivanov VV (2005) Fractal nature of chromatin organization in interphase chicken erythrocyte nuclei: DNA structure exhibits biphasic fractal properties. *FEBS Lett* **579:** 1465–1468

Lenart P, Ellenberg J (2006) Monitoring the permeability of the nuclear envelope during the cell cycle. *Methods* **38:** 17–24

Lieberman-Aiden E, van Berkum NL, Williams L, Imakaev M, Ragoczy T, Telling A, Amit I, Lajoie BR, Sabo PJ, Dorschner MO, Sandstrom R, Bernstein B, Bender MA, Groudine M, Gnirke A, Stamatoyannopoulos J, Mirny LA, Lander ES, Dekker J (2009) Comprehensive mapping of long-range interactions reveals folding principles of the human chromosome. *Science* **326:** 289–293

Lippincott-Schwartz J, Patterson GH (2003) Development and use of fluorescent protein markers in living cells. *Science* **300:** 87–91

Lippincott-Schwartz J, Snapp E, Kenworthy A (2001) Studying protein dynamics in living cells. *Nat Rev Mol Cell Biol* **2:** 444–456

Madden TL, Herzfeld J (1993) Crowding-induced organization of cytoskeletal elements: I. Spontaneous demixing of cytosolic proteins and model filaments to form filament bundles. *Biophys J* **65:** 1147–1154

Marenduzzo D, Finan K, Cook PR (2006) The depletion attraction: an underappreciated force driving cellular organization. *J Cell Biol* **175:** 681–686

Minton AP (1992) Confinement as a determinant of macromolecular structure and reactivity. *Biophys J* **63:** 1090–1100

Minton AP (1995) Confinement as a determinant of macromolecular structure and reactivity. II. Effects of weakly attractive interactions between confined macrosolutes and confining structures. *Biophys J* **68:** 1311–1322

Minton AP (1998) Molecular crowding: analysis of effects of high concentrations of inert cosolutes on biochemical equilibria and rates in terms of volume exclusion. *Methods Enzymol* **295:** 127–149

Minton AP (2006) How can biochemical reactions within cells differ from those in test tubes? *J Cell Sci* **119:** 2863–2869

Misteli T (2005) Concepts in nuclear architecture. *Bioessays* **27:** 477–487

Muramatsu N, Minton AP (1988) Tracer diffusion of globular proteins in concentrated protein solutions. *Proc Natl Acad Sci USA* **85:** 2984–2988

Neale GH, Nader WK (1974) Predictions of transport processes within porous media: creeping flow relative to a fixed swarm of spherical particles. *AIChE* **19:** 530–538

Nemergut ME, Mizzen CA, Stukenberg T, Allis CD, Macara IG (2001) Chromatin docking and exchange activity enhancement of RCC1 by histones H2A and H2B. *Science* **292:** 1540–1543

Netz PA, Dorfmüller T (1995) Computer simulation studies of anomalous diffusion in gels: structural properties and probe-size dependence. *J Chem Phys* **103:** 9074–9082

Pack C, Saito K, Tamura M, Kinjo M (2006) Microenvironment and effect of energy depletion in the nucleus analyzed by mobility of multiple oligomeric EGFPs. *Biophys J* **91:** 3921–3936

Patterson GH, Lippincott-Schwartz J (2002) A photoactivatable GFP for selective photolabeling of proteins and cells. *Science* **297:** 1873–1877

Phair RD, Scaffidi P, Elbi C, Vecerova J, Dey A, Ozato K, Brown DT, Hager G, Bustin M, Misteli T, Cheutin T, McNairn AJ, Jenuwein T, Gilbert DM, Singh PB (2004) Global nature of dynamic protein-chromatin interactions *in vivo*: three-dimensional genome scanning and dynamic interaction networks of chromatin proteins. *Mol Cell Biol* **24:** 6393–6402

Rea S, Eisenhaber F, O'Carroll D, Strahl BD, Sun ZW, Schmid M, Opravil S, Mechtler K, Ponting CP, Allis CD, Jenuwein T (2000) Regulation of chromatin structure by site-specific histone H3 methyltransferases. *Nature* **406:** 593–599

Richter K, Nessling M, Lichter P (2007) Experimental evidence for the influence of molecular crowding on nuclear architecture. *J Cell Sci* **120:** 1673–1680

Richter K, Nessling M, Lichter P (2008) Macromolecular crowding and its potential impact on nuclear function. *Biochim Biophys Acta* **1783:** 2100–2107

Rivas G, Fernandez JA, Minton AP (1999) Direct observation of the self-association of dilute proteins in the presence of inert macromolecules at high concentration via tracer sedimentation equilibrium: theory, experiment, and biological significance. *Biochemistry* **38:** 9379–9388

Rivas G, Fernandez JA, Minton AP (2001) Direct observation of the enhancement of noncooperative protein self-assembly by macromolecular crowding: indefinite linear self-association of bacterial cell division protein FtsZ. *Proc Natl Acad Sci USA* **98:** 3150–3155

Saxton MJ (1993a) Lateral diffusion in an archipelago. Dependence on tracer size. *Biophys J* **64:** 1053–1062

Saxton MJ (1993b) Lateral diffusion in an archipelago. Single-particle diffusion. *Biophys J* **64:** 1766–1780

Sbalzarini IF, Koumoutsakos P (2005) Feature point tracking and trajectory analysis for video imaging in cell biology. *J Struct Biol* **151:** 182–195

Schnell S, Turner TE (2004) Reaction kinetics in intracellular environments with macromolecular crowding: simulations and rate laws. *Prog Biophys Mol Biol* **85:** 235–260

Seksek O, Biwersi J, Verkman AS (1997) Translational diffusion of macromolecule-sized solutes in cytoplasm and nucleus. *J Cell Biol* **138:** 131–142

Shu X, Shaner NC, Yarbrough CA, Tsien RY, Remington SJ (2006) Novel chromophores and buried charges control color in mFruits. *Biochemistry* **45:** 9639–9647

Sprague BL, Muller F, Pego RL, Bungay PM, Stavreva DA, McNally JG (2006) Analysis of binding at a single spatially localized cluster of binding sites by fluorescence recovery after photobleaching. *Biophys J* **91:** 1169–1191

Sprague BL, Pego RL, Stavreva DA, McNally JG (2004) Analysis of binding reactions by fluorescence recovery after photobleaching. *Biophys J* **86:** 3473–3495

Strzelecka TE, Rill RL (1987) Solid-state phosphorus-31 NMR studies of DNA liquid crystalline phases. Isotropic to cholesteric transition. *J Am chem Soc* **109:** 4513–4518

Subirana JA (1990) Analysis of the charge distribution in the C-terminal region of histone H1 as related to its interaction with DNA. *Biopolymers* **29:** 1351–1357

Swamithan R, Hoang CP, Verkman AS (1997) Photobleaching recovery and anisotropy decay of green fluorescent protein GFP-S65T in solution and cells: cytoplasmic viscosity probed by fluorescent protein translational and rotational diffusion. *Biophys J* **72:** 1900–1907

Takahashi M (1989) A fractal model of chromosomes and chromosomal DNA replication. *J Theor Biol* **141:** 117–136

Thévenaz P, Ruttimann UE, Unser M (1998) A Pyramid approach to subpixel registration based on intensity. *IEEE Trans Image Process* **7:** 27–41

Verschure PJ, van der Kraan I, Manders EM, Hoogstraten D, Houtsmuller AB, van Driel R (2003) Condensed chromatin domains in the mammalian nucleus are accessible to large macromolecules. *EMBO Rep* **4:** 861–866

Wachsmuth M, Waldeck W, Langowski J (2000) Anomalous diffusion of fluorescent probes inside living cell nuclei investigated by spatially-resolved fluorescence correlation spectroscopy. *J Mol Biol* **298:** 677–689

Witten TA (1998) Polymer solutions: a geometric introduction. *Rev Mod Phys* **70:** 1531–1544

Woodcock CL, Dimitrov S (2001) Higher-order structure of chromatin and chromosomes. *Curr Opin Genet Dev* **11:** 130–135

Wu J, Berland KM (2008) Propagators and time-dependent diffusion coefficients for anomalous diffusion. *Biophys J* **95:** 2049–2052

Zimmerman SB, Minton AP (1993) Macromolecular crowding: biochemical, biophysical, and physiological consequences. *Annu Rev Biophys Biomol Struct* **22:** 27–65

